# Age-Related Delay in Visual and Auditory Evoked Responses is Mediated by White- and Gray-matter Differences

Price, D.,[1*] Tyler, L. K.,[5] Neto Henriques, R.,[1] Campbell, K.,[2] Williams, N.,[4] Treder, M.,[5] Taylor, J. R.,[3] CamCAN[5] Henson, R. N. A.[1]

1. Medical Research Council, Cognition and Brain Sciences Unit, Cambridge, UK
2. Department of Psychology, Harvard University, USA
3. School of Psychological Sciences, University of Manchester, UK
4. Neuroscience Centre, University of Helsinki, Finland
5. Cambridge Centre for Ageing and Neuroscience, University of Cambridge and MRC Cognition and Brain Sciences Unit, Cambridge, UK

*Corresponding Author:

MRC Cognition & Brain Sciences Unit, 15 Chaucer Road, Cambridge, CB2 7EF, UK
Telephone: +44 1223 355 294
Fax: +44 1223 359 062

**Acknowledgements:** The Cambridge Centre for Ageing and Neuroscience (Cam-CAN) research was supported by the Biotechnology and Biological Sciences Research Council (BB/H008217/1); R.N.H. is additionally supported by the UK Medical Research Council (MC_A060_5PR10). We are grateful to the Cam-CAN respondents and their primary care teams in Cambridge for their participation in this study. We also thank colleagues at the MRC Cognition and Brain Sciences Unit MEG and MRI facilities for their assistance.

**Contributions:** CamCAN conceived the study. CamCAN piloted the study and collected the data. J.R.T., N.W., D.P., and R.H. collated and preprocessed the data. D.P. wrote the in-house MEG analysis software and analysed the data. D.P., R.N.H., L.K.T., N.H., K.C., N.W., M.T., J.R.T. wrote the paper.

# Abstract

Slowing is a common feature of ageing, yet a direct relationship between neural slowing and brain atrophy is yet to be established in healthy humans. We combine magnetoencephalographic (MEG) measures of neural processing speed with magnetic resonance imaging (MRI) measures of white- and gray-matter in a large (N=617, 18-88yrs), population-derived cohort (www.cam-can.org) to investigate the relationship between age-related structural differences and visual and auditory evoked response delay. Using a novel technique, we show that visual-evoked responses exhibit a constant delay, whereas auditory-evoked responses exhibit delay that accumulates over time. Visual delay is mediated by white-matter microstructure in the optic radiation, presumably reflecting increased transmission time, whereas auditory delay is mediated by gray-matter differences in auditory cortex, presumably reflecting less efficient local processing. Our results demonstrate that age has dissociable effects on neural processing speed, and that these effects relate to different types of brain atrophy.

# Introduction

Age-related declines in cognitive abilities like fluid intelligence and working memory are well-documented, and a major burden for both older individuals and the societies they inhabit[1]. One potential common cause for these cognitive declines is a general slowing of information processing speed[2]. This slowing can be measured by behavioural responses in various tasks, and has been related to age-related atrophy of white-matter[3–5] and gray-matter[6–10]. Animal studies have proposed at least two mechanisms of age-related slowing: demyelination, which results in longer axonal transmission times between neurons[11,12], and changes in the neuron itself (such as increased hyperactivity), which results in reduced neural responsiveness[13]. These animal studies reinforce the importance of changes in both white and gray-matter, and raise the possibility that these changes cause different types of neural slowing. Despite these links between white-matter, gray-matter changes and behavioural slowing in humans, and between physiological changes and neural processing delays in animals, there is currently no direct evidence from studies of healthy ageing in humans that links structural brain changes with changes in neural processing speed. Such evidence would provide important mechanistic insights into the causes of age-related slowing of information processing, and hence cognitive decline. We provide this evidence by combining magnetoencephalography (MEG) and magnetic resonance imaging (MRI) from a large sample of 617 population-derived healthy adults, distributed uniformly from 18-88 years of age, recruited from the Cambridge Centre for Ageing and Neuroscience (CamCAN) (www.cam-can.org).

Age-related slowing of the neural response evoked by simple visual stimuli such as checkerboards has been observed using event-related potentials (ERPs) recorded with electroencephalography (EEG)[14–17]. Similar effects have also been found for auditory stimuli[18–20], and for complex visual stimuli such as faces[21–25]. Some studies have reported effects of age on early components of the ERP/ERF (e.g. within 200ms of stimulus onset)[14,26], while others have reported effects that affect later components, typically 200-800ms, without a corresponding increase in latency in the early components[18,22,24,25,27–29]. We propose that these reflect two distinct types of delay: constant and cumulative delay. Constant delay affects all time-points equally, equivalent to a temporal shift of the whole evoked response (both early and late components). Cumulative delay, on the other hand, increases with post-stimulus time, and therefore is easier to detect for late than early components. Despite several reports of cumulative delay in the literature[18,22], there has been no systematic comparison of constant and cumulative delay, and it is possible that they have different neuronal causes.

The study of age-related delays in ERPs/ERFs is further complicated by inconsistent findings in the degree of age-related delay of both early and late components (for review, see [14,24–26]). There are several likely sources of this inconsistency. Firstly, differences in information processing demands across experimental tasks (such as attending to faces versus ignoring auditory oddballs) makes evoked responses difficult to compare across studies. While clearly providing important information in their respective domains, complex tasks like face recognition are likely to recruit multiple cortical systems, and it is unclear how each system contributes to the spatially-integrated signal recorded by EEG/MEG. Secondly, age-related delays may differ according to the type of stimulus, for example visual versus auditory stimuli, because age could potentially have differential effects on brain regions specialised for different sensory modalities. Even when results are consistent across different tasks and modalities, they are rarely compared directly within the same group of participants. Thirdly,

previous studies have tended to compare small groups of young versus old volunteers, rather than examine continuous differences across the adult lifespan, and tended to use volunteers who are self-selecting, rather than being representative of the population.

Yet another important source of inconsistency across studies is the method of measuring delay. One common measure is the latency of the peak (maximum) of an evoked component. This measure is very sensitive to noise however (being based on a small number of time points), so other techniques pool over several time points[22], for example using the fractional area latency[30], or the slope or intercept of best-fitting functions. Here we use all (peristimulus) time-points to estimate delay, improving robustness and sensitivity, and enabling estimation of second-order delay characteristics like constant and cumulative delay, which are not readily available from single peak latencies, and difficult to quantify when there are multiple, potentially overlapping temporal components.

To address these limitations in the literature, we directly compared the effects of age across two types of task (passive and active), on both visual and auditory stimuli. We applied our novel method for simultaneously estimating constant and cumulative delay to a larger and more representative (opt-out) sample than typically tested, which spanned the whole adult lifespan. Furthermore, we related these estimates of neural delay, for the first time, to structural estimates of both gray-matter and white-matter on the same individuals.

More precisely, we used simple stimuli (visual checkerboards and pure tones) that are likely to activate only a few brain regions, and compared two tasks that differed in attentional demand: i) a "passive" viewing/listening task in which visual or auditory stimuli were presented separately, and did not require a response, and ii) an "active" task in which the same stimuli were presented simultaneously, and required a motor response. We also used MEG, which has the same temporal resolution as the EEG used in most previous studies, but has the advantage of higher spatial resolution, owing to the fact that magnetic fields are less susceptible than electrical fields to spatial distortion in biological tissue[31], thereby increasing our ability to separate brain sources (see also[25]). The measures of brain structure came from three types of MRI contrast: T1-weighted, T2-weighted and diffusion-weighted. The T1 and T2 data were combined in order to optimise estimation of local gray-matter (GM) volume. Diffusion data were optimised for estimation of the mean kurtosis (MK) of the tissue's water diffusion[32,33], which is believed to offer a sensitive metric of age-related changes of white-matter microstructure, such as changes of cell membranes, organelles and the ratio of intra and extra-cellular water compartments[34]. Moreover, in contrast to standard diffusion tensor measures, diffusion kurtosis measures are robust to regions with a high concentration of crossing fibres[33,35].

Our main experimental hypotheses were that age is positively correlated with constant and/or cumulative evoked response delay in auditory and visual conditions, and that this relationship between age and delay is mediated by differences in white-matter microstructure or gray-matter volume.

# Results

## *PCA-Derived Event Related Fields*

We start with data from the passive task, in which auditory tones and visual checkerboards were presented in separate trials. In order to reduce our dataset to a small set of meaningful components and improve the signal-to-noise ratio, principal component analysis (PCA) was performed on the trial-averaged event-related fields (ERFs) for each stimulus-type, after concatenating the data in the time dimension (see online Methods). The first principal component entailed a single spatial component for all participants (Fig. 1a), a separate time-course for each participant (Fig. 1c), from which an average time-course was derived for the entire age-range (Fig. 1d). We used multiple sparse priors (MSP)[36] to localise the spatial component, which revealed a single peak in bilateral primary auditory cortex for the auditory stimuli and in bilateral extrastriate cortex for the visual stimuli (Fig. 1a-b). Importantly, the ERP-images in Figure 1c show how the ERFs are delayed as age increases, with indication of a cumulative shift for auditory stimuli and a constant shift for visual stimuli; a difference that we formally quantify below.

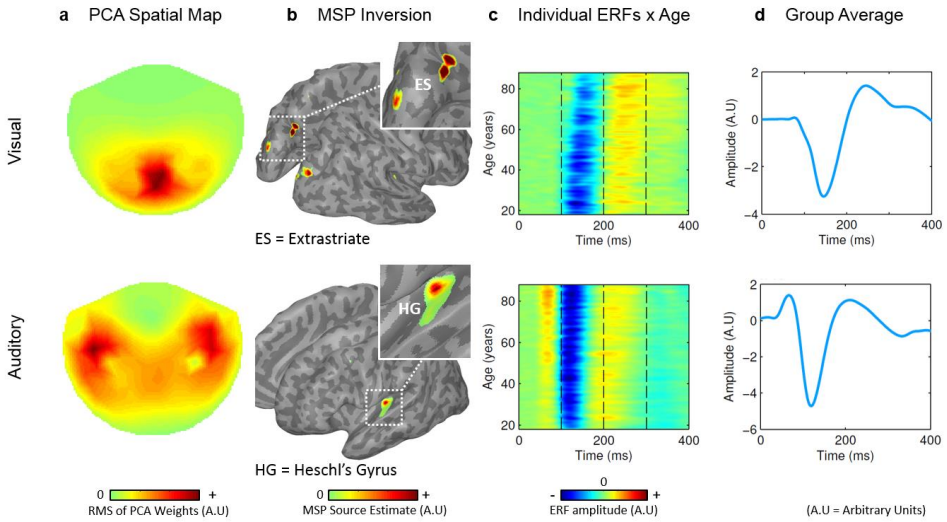


**Figure 1**. (a) 2D topographical MEG sensor plot of the first spatial component derived using PCA. Values represent the root mean square (RMS) of each pair of gradiometers. (b) Group MSP source reconstruction based on the spatial component shown in **a** (cluster peak MNI coordinates: right HG = 38, -22, 8; left = -38, -26, 8; right V2 = 14, -96, 20; left = -14, -96, 20; ES right = 16, -74, 24; L = -16, -74, 20). (c) Heat-maps illustrating the time-courses for each participant from the first temporal component of the PCA. Data are smoothed in the y-direction for visualisation only (FWHM = 5 subjects). (d) Group average time-courses (also used as the template for delay estimation).

### *ERF Fitting of Principal Component Time-Courses*

In order to estimate constant and cumulative delay for each participant, a template fitting procedure was employed, in which the group average signal (Fig. 1d) was fit to each participant's ERF by a combination of temporal displacement (constant delay) and temporal linear dilation (cumulative delay). These two parameters were adjusted until the model fit ($R^2$) was maximised (after which an estimate of amplitude scaling was also obtained; see online Methods).

Constant and cumulative delay estimates for the audio and visual ERFs were correlated with age, using robust regression after removing outlying values for each modality separately (Fig. 2). In the visual condition, there was a significant effect of age on constant delay ($R^2$=0.10, p<0.001, N=505), but no effect of age on cumulative delay ($R^2$=0.00, p=0.99, N=505). In the auditory condition, on the other hand, there was a significant effect of age on cumulative delay ($R^2$=0.15, p<0.001, N=572), but not on constant delay ($R^2$=0.00, p=0.90, N=572).

We also repeated the PCA and ERF fitting steps for the active task, in which the auditory and visual stimuli were presented simultaneously, and to which the participant responded with a key-press. This PCA produced similar results (Supplementary Fig. 1), while the latency results are shown in Supplementary Figure 1B, where it can be seen that the same pattern of age effects emerged. Note that, for both passive and active tasks, the next strongest principal components (PCs 2-5) showed either similar patterns, or no apparent delay with age (see Supplementary Fig. 2). Moreover, PC1 accounted for 48% and 28% of the variance of the ERFs across all participants for passive auditory and visual conditions respectively. By comparison, PC2 accounted for 9% and 12% respectively. Therefore, we used only the first principal component for subsequent analyses.

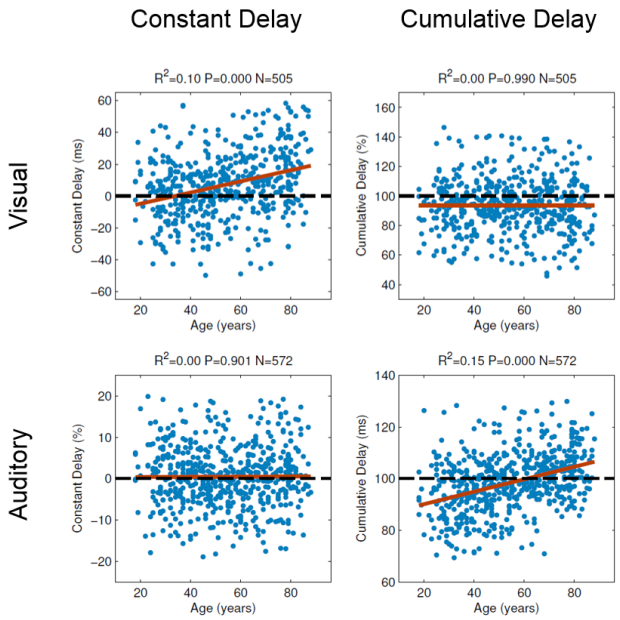


**Figure 2.** ERF fitting results. Robust regressions with age. There is a significant effect of age on constant but not cumulative delay in the visual ERFs and a significant effect of age on cumulative but not constant delay in the auditory ERFs.

*Adjusting for sensory acuity, fit amplitude and fit error*

It is possible that these effects of age on neural delays are simply a consequence of the known age-related changes in sensory acuity (despite our screening criteria, and use of lenses to correct vision; see online Methods). We therefore correlated the neural delay estimates against separate, standardised measures of auditory and visual thresholds (see online Methods), as shown in Supplementary Figure 3. There was a weak negative relationship between visual acuity and visual constant delay ($R^2$=0.01, P=0.007, N=504), though this effect disappeared after adjusting for age ($R^2$=0.00, P=0.983, N=504). Similarly, auditory acuity was weakly negatively related to auditory cumulative delay ($R^2$=0.05, P<0.001, N=504), but not after adjusting for age ($R^2$=0.00, P>0.05, N=504). Importantly however, both visual and auditory age-related neural delays remained significant after controlling for visual ($R^2$=0.08, P<0.001, N=505) and auditory ($R^2$=0.09, P<0.001, N=570) sensory acuity, respectively.

To check that the effects of age on neural delay estimates were not biased by effects of age on the estimated response amplitude or the estimated fit quality, we repeated the partial correlation of neural delays with age after adjusting for these estimates too. Finally, for both visual and auditory measures, the effects of amplitude on delay were uncorrelated after controlling for age and the effects of age on delay remained highly significant after controlling for amplitude (visual constant, $R^2$=0.10, P<0.001, N=505; auditory cumulative, $R^2$=0.15, P<0.001, N=572, Supplementary Fig. 4). The same statement was true for fit error (visual constant, $R^2$=0.09, P<0.001, N=505; auditory cumulative, $R^2$=0.16, P<0.001, N=572, Supplementary Fig. 5). Thus, there is no evidence our age-related neural delays were caused by age-related differences in sensory acuity, response amplitude or model fit.

In summary, it appears that age has a qualitatively different effect on neural delay in auditory and visual modalities. Indeed, the auditory cumulative delay was only weakly correlated with visual constant delay ($R^2$=0.01, p=0.007, N=519), and this effect vanished when controlling for age ($R^2$=0.00, p=0.829, N=519), suggesting these two delay parameters are not intrinsically related, and are therefore likely to have separate underlying causes. To investigate these causes, we turned to the MRI data on each participant.

*Mediation of Neural Latency by Structural Brain Measures*

In order to test the hypothesis that brain structural changes account for some of the shared variance between age and neural delay, whole-head voxel-wise robust mediation analyses were performed, using the M3 Mediation Toolbox[37]. Mediation analysis tests whether the relation – path c – between a predictor variable (X, age) and an outcome variable (Y, ERF delay) is significantly attenuated when the relation between X and a mediator variable (M, white-matter microstructure or gray-matter volume) – path a – and the relation between M and Y – path b – are added to the model. Four separate, whole-brain voxel-wise mediation models were tested: one for each type of delay (auditory cumulative or visual constant) as the outcome and each brain measure (white- or gray-matter) as the mediator. All models included total intracranial volume (TIV) as a covariate of no interest. Mediation effect sizes were computed for every voxel, and a false detection rate (FDR) cluster extent threshold of 5% applied in order to correct for multiple comparisons across voxels. This threshold was further Bonferroni-corrected for multiple comparisons across the four models. Finally, voxels were also required to i) be positive, meaning that the age vs. delay relationship is attenuated by the mediator, ii) show significant relations between age and mediator (path a) and between mediator and outcome (path b) after the same FDR correction, and iii) fall within gray-matter or white-matter masks. Finally, clusters of voxels below the cluster levels thresholds were also excluded (see online Methods).

The mediation effects of white-matter microstructure on the age versus visual constant delay relationship are displayed in Figure 3a. Significant clusters of mediation effects were found in the left retrolenticular part of the internal capsule (RIC), and the right posterior thalamic radiation (PTR). These paths together form the optic radiation projecting from the lateral geniculate nucleus (LGN) to the primary visual cortex (V1). The cluster centred on left RIC extended to left superior corona radiata and left superior longitudinal fasciculus, although the mediation effects here were generally lower. The cluster visible in right PTR also extended to splenium of corpus callosum (connecting left and right visual cortices).

Mediation effects of white-matter on the age vs. auditory cumulative delay relationship are displayed in Figure 3b. One cluster was found with a peak close to the corpus callosum, which contains interhemispheric connections between left and right auditory cortex[38].

Mediation effects of gray-matter on the age vs. auditory cumulative delay relationship are displayed in Figure 3c. A significant cluster was found comprising the left posterior superior temporal sulcus (STS), extending to middle temporal gyrus (MTG). There was no evidence that gray-matter mediated the effects of age on visual constant delay.

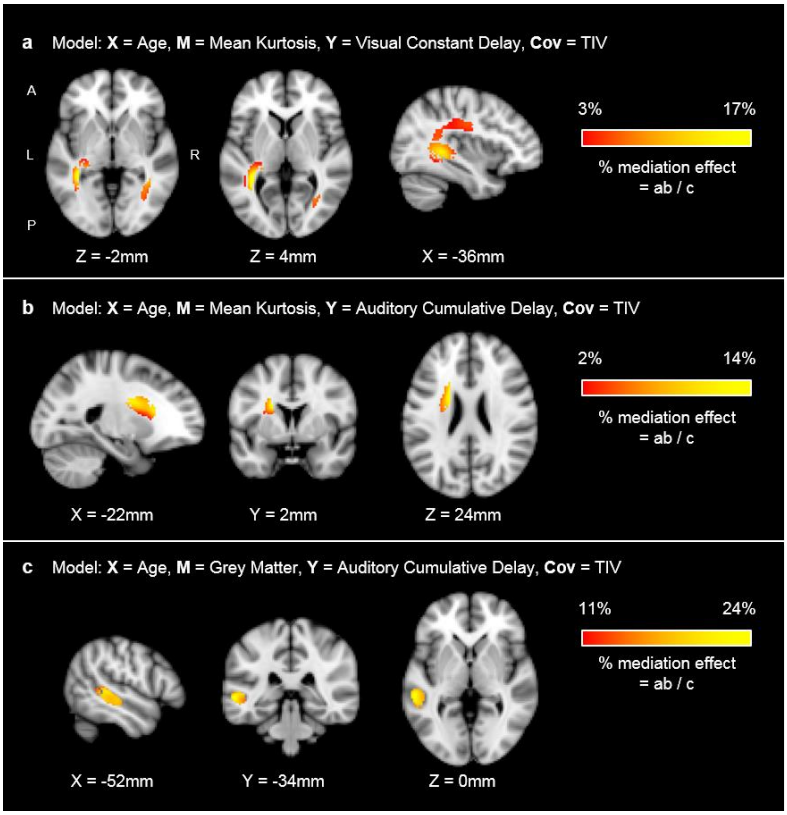


**Figure 3**. Whole-brain voxel-wise mediation analysis results. Only those clusters surviving whole-brain correction shown. (a) WM structure (mean kurtosis, MK) in the optic radiation (connecting LGN to V1) mediates the age vs. visual constant delay relationship. (b) MK in the superior corona radiata mediates the age vs. auditory cumulative delay relationship. (c) GM volume in the left posterior superior temporal sulcus (STS) mediates the age vs. auditory cumulative delay relationship. All effects indicate positive mediation (i.e., the age vs. delay relationship is attenuated when including the mediator).

# Discussion

Using a novel analysis technique on MEG data from a large, lifespan cohort, we discovered two distinct types of age-related neuronal delays in sensory evoked responses: a constant delay in the visual response to checkerboards and a cumulative delay in the auditory response to tones. These delays occurred regardless of whether participants were passively encountering auditory and visual stimuli separately, or actively responding to them when the stimuli were presented concurrently, suggesting that these age effects occur under both low and high levels of attention. After controlling for common age effects, these two types of delay were uncorrelated across individuals, suggesting dissociable causes. In support of this, we found that white-matter microstructure (mean kurtosis, MK, from diffusion-weighted MRI) in the optic radiation (LGN to V1) mediated the effect of age on the visual constant delay, whereas gray-matter volume (as estimated from T1- and T2-weighted MRIs) in the posterior superior temporal sulcus (STS), as well as white-matter microstructure near inter-hemispheric fibre bundles, mediated the effect of age on the auditory cumulative delay. We discuss these findings in light of prior behavioural, neuroimaging and animal studies.

## *Visual Constant Delay*

The age-related neural slowing in the visual ERF and its relationship to white-matter microstructure in the optic radiation point to a delay in the arrival time of information communicated from the LGN to V1. Several aspects of our results support this conclusion. Firstly, the main generator of the visual ERF was located in the extrastriate visual cortex. Secondly, the slowing was characterised by a constant delay of the entire ERF, so that both early (~50-200ms) and late (~200-500ms) components of the evoked response were affected, consistent with a delayed arrival time. Thirdly, the whole-brain voxel-wise mediation analysis revealed that microstructural differences in the left retrolenticular internal capsule (RIC) and right posterior thalamic radiation (PTR) partially account for the age-related delay. The RIC in particular is a major junction of fibres that transmit information from the LGN to visual cortex (and our use of diffusion kurtosis likely increased our sensitivity to regions with such crossing or fanning fibres). Furthermore, the lack of a cumulative delay suggests that, once the information reaches visual cortex, it is processed at a normal rate (cf. auditory results below).

These results contrast with findings in the senescent macaque monkey, which revealed no white-matter atrophy, and instead spike timing delays were related to increased neuronal excitability[13]. This highlights the importance of investigating ageing *in-vivo* in humans, who may have different neurobiological ageing profiles to animals. These results do not preclude the possibility that other information-carrying fibres and thalamic nuclei play a role in visual processing delays, but it is clear that age-related differences in white-matter microstructure are partially responsible for delay of information processing in healthy human ageing.

## *Auditory Cumulative Delay*

The age-related cumulative delay observed in the auditory evoked response, along with the lack of constant delay, points to a different mechanism than that associated with the visual response. We suggest that this cumulative delay reflects a deficit in local processing within auditory cortex, specifically recurrent interactions between primary auditory cortex and higher order auditory regions. We again base this claim on several aspects of our analysis. Firstly, the main source of the auditory ERF was the primary auditory cortex, in-line with evidence that this region responds to pure tones[39]. This delay was mediated by gray-matter volume in a higher order auditory region, namely the superior temporal sulcus (STS). The STS is too distant from the primary source to be considered the generator of the ERF, but is certainly anatomically connected to primary auditory cortex[40], suggesting that interactions with STS are responsible for the temporal dilation of the primary auditory response. Indeed, the auditory system is organised into a functional hierarchy, beginning with processing of simple sounds (tone and frequency) in primary auditory cortex, before further processing in surrounding "belt" regions in the superior temporal lobe[39], including STS. Importantly, early processing in the primary sensory regions is known to be modulated by top-down inhibitory processes[41,42]. The cumulative delay observed in the present study may therefore be linked to a disruption of dynamic inhibitory interactions between primary auditory cortex and higher processing regions, resulting in delay that worsens over the duration of the evoked response, but does not affect the arrival time of information to the cortex from thalamic nuclei.

We also found that MK in a cluster with a peak near the corpus callosum mediated the age-related differences in auditory cumulative delay. The mechanistic relationship between delay and structural differences is less clear in this case, but one possibility is that additional breakdown of interactions between left and right auditory cortices results in further delay even after initial thalamic input has reached each hemisphere. Indeed, it is possible that loss of white-matter tracts like these result in cascading denervation of higher auditory gray-matter structures (e.g. STS) and less efficient interactions with primary auditory regions[43].

## *Sensory Acuity*

One potential alternative cause of age-related delay in evoked responses is the well-known age-related change in sensory acuity. If sensory acuity were an adequate predictor of neural delay, we would expect a relationship between acuity and delay to remain even after adjusting for age. However, while auditory acuity was weakly correlated with auditory cumulative delay, when accounting for age, this correlation disappeared. The same was true for the relationship between visual acuity and visual constant delay. Most importantly, the correlation between delay and age remained significant after adjusting for sensory acuity. These results suggest that sensory acuity does not play a significant role in our findings, which is consistent with other studies arguing that visual acuity cannot fully account for age-related delays in the visual evoked response[15–17,21].

*Caveats*

While our results go beyond previous studies in testing for age-related delays across both visual and auditory modalities and across two different tasks, our findings are nonetheless restricted to simple visual and auditory stimuli, which may not generalise to more complex stimuli that require more extensive neural processing. This might explain the age-related cumulative delay found previously in the ERP to faces[22], which likely involves a greater degree of recurrent processing between multiple visual cortical regions responsible for face perception.

Secondly, caution is warranted over interpretation of our mediation analysis. Mediation analysis is a statistical approach that cannot properly determine causality in the same way that an intervention might (e.g., to lesion parts of the optic radiation and test effects on visual constant delay). Furthermore, mediation results from cross-sectional studies cannot be interpreted solely in terms of the ageing process[44], and have alternative explanations such as cohort effects. Whatever the precise role of age, our findings nonetheless demonstrate that there are at least two types of neural processing delay, which are unrelated across individuals, and have different relationships with white- and gray-matter in the brain structures associated with that processing.

Finally, note that we are not claiming that our present white- and gray-matter findings are a complete account of age-related slowing. Our mediation effect sizes in any voxel explained at most 24% of the age-related variance in response delays. It is possible that a larger proportion of variance in neural delay could be explained by combining brain measures across voxels, but even then, full mediation would be surprising since several other factors not measured here, such as neurotransmitter concentrations, are also likely contributory factors. Nonetheless, our findings represent a considerable step forward in demonstrating dissociable types of age-related neuronal slowing, and generating mechanistic hypotheses for their causes.

*Conclusion*

In summary, the present work fills a long-sought missing gap in the literature: evidence that in healthy humans, age-related delay of the electrophysiological response to stimulation is due to structural differences of functionally relevant brain regions responsible for the transfer and processing of information. We have taken this a step further to show that neural delay should not be thought of as a unitary concept that affects all brain regions equally. Instead, ageing is associated with regionally specific changes in characteristic neural responses, which are likely due to heterogeneous age-related changes across anatomical structures.

# Methods

*Participants*

Participants were recruited from a healthy population-derived sample from the Cam-CAN study (www.cam-can.org; see Shafto et al.[45] for a comprehensive explanation of the study design and experimental protocol). Ethical approval for the study was obtained from the Cambridgeshire Research ethics committee. Prior to the home interview, individuals give written informed consent for the study. Written informed consent is also given by participants at each scanning session. Participants were excluded based on several criteria: Mini Mental State Examination (MMSE) < 25; failing to hear a 35dB 1kH tone in either ear; poor English language skills (non-native or non-bilingual speakers); self-reported substance abuse and serious health conditions (e.g. major psychiatric conditions, or a history of stroke or heart conditions); or MRI or MEG contraindications (e.g. ferromagnetic metallic implants, pacemakers, or recent surgery). Participants that did not take part in both the MEG and MRI sessions were also excluded. The final sample of N=617 had an age range of 18-88 years at the time of first contact. Participants took both a visual and auditory acuity test immediately preceding the MEG scan. The scores from these tests were also used in later statistical analysis of age-related neural delay to control for the possible confounds of age-related differences of visual/auditory acuity (2 participants with missing acuity data were removed).

*MRI Data*

MRI data were acquired using a Siemens 3T TIM TRIO (Siemens, Erlangen, Germany) with a 32-channel head coil at the MRC Cognition & Brain Sciences Unit (CBU), Cambridge, UK. Anatomical images were acquired with a resolution of 1mm$^3$ isotropic using a T1-weighted MPRAGE sequence (TR: 2250ms; TE: 2.98ms; TI: 900ms; 190Hz; flip angle: 9°; FOV: 256 × 240 × 192mm; GRAPPA acceleration factor: 2; acquisition time of 4 minutes and 32 seconds), and a 1mm$^3$ isotropic T2-weighted SPACE sequence (TR: 2800ms; TE: 408ms; flip angle: 9°; FOV: 256 × 256 × 192mm; GRAPPA acceleration factor: 2; acquisition time of 4 minutes and 32 seconds). Diffusion-Weighted Images (DWIs) were acquired with a twice-refocused spin-echo sequence, with 30 diffusion gradient directions for each of two b-values: 1000 and 2000 s/mm$^2$, plus three images acquired with a b-value of 0. These parameters are optimised for estimation of the diffusion kurtosis tensor and associated scalar metrics. Other DWI parameters were: TR=9100 milliseconds, TE=104 milliseconds, voxel size = 2mm isotropic, FOV = 192mm x 192mm, 66 axial slices, number of averages=1; acquisition time of 10 minutes and 2 seconds.

All MRI data were analysed using the SPM12 software (www.fil.ion.ucl.ac.uk/spm), implemented in the AA 4.2 batching software (https://github.com/rhodricusack/automaticanalysis; for complete description of data and pipelines, see Taylor et al.[46]).

The T1 and T2 images were initially coregistered to the MNI template using a rigid-body transformation, and then combined in order to segment the brain into 6 tissue classes: GM, WM, cerebrospinal fluid (CSF), bone, soft tissue, and residual noise (Ashburner & Friston, 2005). The GM images were then submitted to diffeomorphic registration (DARTEL; Ashburner, 2007) to create group template images, which was then affine-transformed to the MNI template. To accommodate changes in volume from these transformations, the GM images were modulated by the Jacobean of the deformations to produce estimates in MNI space of the original local GM volume.

The DWI data were first coregistered with the T1 image and then skull-stripped using the BET utility in FSL (http://fsl.fmrib.ox.ac.uk/fsl/fslwiki/). Linear fitting of a higher-order tensor was then used to estimate mean kurtosis (using in-house code). Images of the diffusion metrics were then normalised to MNI space using the DARTEL+affine transformations from the T1+T2 pipeline above.

### *MEG Scanning and Pre-processing*

Data were collected continuously using a whole-head Elekta Neuromag Vector View 306 channel MEG system (102 magnetometers and 204 planar gradiometers) (Elekta, Neuromag, Helsinki, Finland), located in a light magnetically shielded room (MSR) at the CBU. Data were sampled at 1kHz with a highpass filter of 0.03Hz. Recordings were taken in the seated position. Head position within the MEG helmet was estimated continuously using four Head-Position Indicator (HPI) coils to allow for offline correction of head motion. Two pairs of bipolar electrodes were used to record vertical and horizontal electrooculogram (VEOG, HEOG) signals to monitor blinks and eye-movements, and one pair of bipolar electrodes to record the electrocardiogram (ECG) signal to monitor pulse-related artefacts. Instructions and visual stimuli were projected onto a screen through an aperture in the front wall of the MSR. Participants were given MEG-compatible glasses to correct their vision. Auditory stimuli were presented binaurally via etymotic tubes. Motor responses were made via a custom-built button box with fibre optic leads.

Temporal signal space separation (tSSS; MaxFilter 2.2, Elekta Neuromag Oy, Helsinki, Finland) was applied to the continuous MEG data to remove noise from external sources and from HPI coils (correlation threshold 0.98, 10-sec sliding window), for continuous head-motion correction (in 200-ms time windows), and to virtually transform data to a common head position ('-trans default' option with origin adjusted to the optimal device origin, [0, +13, -6]). MaxFilter was also used to remove mains-frequency noise (50-Hz notch filter) and to automatically detect and virtually reconstruct any noisy channels. Data were then imported into Matlab using SPM12. ICA was used to identify physiological artefacts from blinks, eye-movements, and cardiac pulse. This was done by identifying those ICs whose time courses and spatial topographies correlated highly with reference time courses (correlation greater than three standard deviations from mean) and spatial topographies (correlation greater than two standard deviations from mean), respectively, for each of the above artefact types (run via in-house code, "detect_ICA_artefacts.m" available from http://www.mrc-cbu.cam.ac.uk/people/rik.henson/personal/analysis/).

Data were then filtered using a two-pass Butterworth filter (1-32Hz), epoched (time window: -100-500ms post stimulus onset), and the average baseline (-100-0ms) was subtracted from the data. Trial averaged responses of evoked amplitude were computed for each channel, participant and condition of the experiment. This resulted in a 2-dimensional matrix for each participant (channels x time). All subsequent analyses were carried out using data from the 204 gradiometer channels, since these are more sensitive to superficial sources than the magnetometer sensors, and the sensory cortices of interest here are superficial. ERP fitting on both the passive and task sessions was performed on the principal components of the channel level data (see *PCA based latency analysis* below).

### *Audio / Visual Tasks*

The visual stimulus consisted of two circular checkerboards visually presented simultaneously to the left and right of a central fixation cross (34ms duration x 60 presentations). The auditory stimulus was a binaural tone (300ms duration; 20 presentations of 300Hz, 600Hz, and 1200Hz; 60 total presentations).

The first session involved the active task, in which participants were presented with both types of stimuli concurrently, and asked to respond by pressing a button with their right index finger immediately after stimulus onset. The stimulus-onset asynchrony varied randomly between 2s and 26s, to match an fMRI version of same task (see Taylor et al.[46] for more details). The session lasted 8min and 40s in total.

The second session was the passive task. Participants experienced separate trials with either the visual or auditory stimulus, which they were asked to passively observe (no response required). Visual and auditory trials were pseudo-randomly ordered, with an SOA that varied randomly between from 0.9s to 1.1s. The session lasted approximately 2mins.

### *PCA Based Latency Analysis*

The 2D (time x sensor) matrices for each participant were concatenated along the time dimension. PCA was performed with columns as signals and rows as observations to produce a set of time domain signals for each trial-type. The $n^{th}$ principal component was then reshaped to give individual trial averages for each participant. The principal component weights represent the degree to which each channel contributes towards the $n^{th}$ principal component. Given that the relationship is linear, the weights can also be used for source localisation. Since the simple sensory-evoked sources are likely to be distributed across multiple regions, we used multiple sparse priors (MSP), implemented in SPM12, which is capable of recovering multiple sparsely distributed generators of ERFs[36]. Each participant's MRI was coregistered to their MEG data using three anatomical fiducial points (nasion, and left and right pre-auricular points) that were digitised for the MEG data and identified manually on the MRIs. Lead fields were calculated using a single-shell model based on the deformed spheres approach[47].

### *ERP Fitting*

The aim of the fitting procedure was to obtain estimates for two types of delay: constant delay, defined as delay that affects all time points equally (modelled using a $0^{th}$ order delay parameter); and cumulative delay, defined as delay that is linearly dependent on the time point at which it is measured (modelled using a $1^{st}$ order delay parameter). Note that the delay terms could be of any order, but limiting the delay estimates to $0^{th}$ and $1^{st}$ order terms reduces the danger of over-fitting. ERP fitting was performed using in-house code written in MATLAB. Firstly, a template ERF was computed from the data as the trial-

averaged ERF for a given principal component, averaged across all participants. Because this template represents the group average, approximately equal numbers of participants will have negative as positive delay parameters when fitting their individual ERFs. A template fitting algorithm was designed to iteratively alter the temporal characteristics of the template signal $\boldsymbol{s}$ by:

$$\hat{\boldsymbol{s}}(t, t_0, \tau_{CUM}, \tau_{CON}) = \boldsymbol{s}(t - \tau_{CON} - [t - t_0]\tau_{CUM}).$$

where $\tau_{CON}$ is the constant delay, $\tau_{CUM}$ is the cumulative delay and $t_0$ is a stationary point in time for any value of $\tau_{CUM}$, and was constant across all tests (see below). Cubic spline interpolation was used to obtain $\hat{\boldsymbol{s}}$ for any given set of delay parameters.

*Fitting Procedure*: For each individual time-course $\boldsymbol{s}$, the parameters were adjusted iteratively using a gradient descent algorithm until the convergence criteria was satisfied. Starting parameters were chosen to correspond to the null hypothesis that no delay would be observed compared to the group average ($\tau_{CON} = 0$; $\tau_{CUM} = 1$), and delay parameters were adjusted by a predefined quantity ( $\tau_{CON} = +/-20ms$; $\tau_{CUM} = +/-10\%$), giving 4 fits per iteration. A value of $t_0 = 75ms$ was fixed on the basis of the typical latency for information to reach sensory cortices. Fit was determined using linear regression, and the parameter values that gave the best $R^2$ fit were chosen as starting points in the next iteration. Using regression simplified the fitting procedure, since amplitude scaling and mean were determined from the regression model's beta estimate and intercept, respectively. If none of the parameters resulted in a better fit than the current best fit, then the magnitude of the parameter adjustments were reduced by a factor of 0.75 and the process was repeated. Convergence was achieved when the $R^2$ fit improvement over the current best fit was less than 1e-5. This method helped to reduce the occurrence of spurious outliers, because the gradient descent was constrained to converge into the maxima closest to the starting point. Results were visually inspected to ensure optimal fitting was achieved. Outlier parameter values were handled during statistical testing, described below.

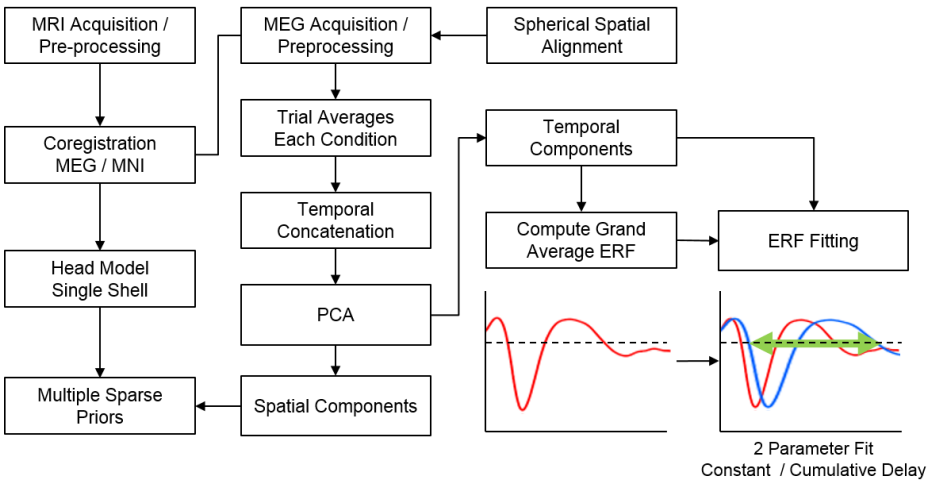


**Figure 4**: Flow chart diagram illustrating the processing steps involved in the analysis of MEG data.

*Robust Regression*

For each delay parameter, outliers were identified based on the boxplot rule (+/- 1.5 times the inter-quartile range, IQR) and removed from the analysis. An outlier in either the constant or cumulative delay estimate resulted in the participant being rejected from the analysis for a given experimental condition (visual or auditory). For all correlation analyses, robust methods were employed to control for remaining extreme values, and for any non-normally distributed data. Robust regression was implemented using MATLAB Statistical Toolbox. A bi-square weighting function with a tuning constant of 4.685 was used to weight cases based on their residual error from an ordinary least squares fit, then repeated until convergence.

*Whole-Brain Voxel-Wise Mediation Analysis*

Images in MNI space of Mean Kurtosis (MK) from the DWI pipeline, and of local gray-matter volume (GMV) from the T1 and T2 pipeline, were entered into a whole-brain voxel-wise robust mediation analysis implemented using the M3 Mediation Toolbox (http://wagerlab.colorado.edu)[37]. A three path model was used with age as the predictor variable (X), delay as the dependent variable (Y) (outliers removed as above), and anatomical data as the mediator variable (M). Since total intracranial volume (TIV) was correlated with age ($R^2$ = 0.01, p=0.03), it was also included as a covariate to control for the possible confounding effects of head size on structural statistics.

Mass univariate robust mediation was computed per voxel using the "robust fit" option of the M3 toolbox (10,000 bootstrapped samples per voxel) to generate path data (paths: a = X->M, b = M->Y, c' = X->Y, c = ab+c'), and associated p-values calculated per voxel. The

bootstrapping method, which involves resampling the data to generate a null distribution of statistical results and hence a p-value for the observed mediation effect, is more robust to outliers and non-normally distributed data. Four models were tested, all with age as the predictor (X) and TIV as covariate of no interest, which correlated with age ($R^2$=0.01, p=0.03, N=617). The mediator variable (M) was voxel data from either the white or gray-matter images. White-matter volumes were masked using the JHU ROIs (all ROIs were included); gray-matter volumes were masked using the Harvard Oxford gray-matter atlas. Only those voxels falling within the mask were entered into the mediation model. The false detection rate (FDR) threshold for each image was calculated from the resulting p-value maps using the M3 mediation toolbox. Statistical maps were thresholded according to these p-value thresholds. Clusters below a certain size threshold were then excluded. Cluster size thresholds were different for white (N voxels = 50) and gray-matter (N voxels = 250) because white-matter masks tended to contain narrow paths, particularly in the optic radiation. Mediation effect sizes were calculated using the formula, $M_{effect} = 100ab/c$, which represents the mediation effect on the c path of including M in the model (resulting in c') as a percentage of the total direct effect (c). A value of 100% indicates full mediation.

# References


1. Kievit, R. A. *et al.* Distinct aspects of frontal lobe structure mediate age-related differences in fluid intelligence and multitasking. *Nat. Commun.* **5,** (2014).
2. Salthouse, T. A. The processing-speed theory of adult age differences in cognition. *Psychol. Rev.* **103,** 403 (1996).
3. Lu, P. H. *et al.* Age-related slowing in cognitive processing speed is associated with myelin integrity in a very healthy elderly sample. *J. Clin. Exp. Neuropsychol.* **33,** 1059–1068 (2011).
4. Lu, P. H. *et al.* Myelin breakdown mediates age-related slowing in cognitive processing speed in healthy elderly men. *Brain Cogn.* **81,** 131–138 (2013).
5. Thomas, C. *et al.* Reduction in white matter connectivity, revealed by diffusion tensor imaging, may account for age-related changes in face perception. *J. Cogn. Neurosci.* **20,** 268–284 (2008).
6. Chee, M. W. *et al.* Cognitive function and brain structure correlations in healthy elderly East Asians. *Neuroimage* **46,** 257–269 (2009).
7. Eckert, M. A. Slowing down: age-related neurobiological predictors of processing speed. *Front Neurosci* **5,** 1–13 (2011).
8. Eckert, M. A., Keren, N. I., Roberts, D. R., Calhoun, V. D. & Harris, K. C. Age-related changes in processing speed: unique contributions of cerebellar and prefrontal cortex. *Front. Hum. Neurosci.* **4,** 10 (2010).
9. Kennedy, K. M. & Raz, N. Age, sex and regional brain volumes predict perceptual-motor skill acquisition. *Cortex* **41,** 560–569 (2005).
10. Schretlen, D. *et al.* Elucidating the contributions of processing speed, executive ability, and frontal lobe volume to normal age-related differences in fluid intelligence. *J. Int. Neuropsychol. Soc.* **6,** 52–61 (2000).
11. Peters, A. The effects of normal aging on myelin and nerve fibers: a review. *J. Neurocytol.* **31,** 581–593 (2002).
12. Xi, M.-C., Liu, R.-H., Engelhardt, J. K., Morales, F. R. & Chase, M. H. Changes in the axonal conduction velocity of pyramidal tract neurons in the aged cat. *Neuroscience* **92,** 219–225 (1999).
13. Wang, Y., Zhou, Y., Ma, Y. & Leventhal, A. G. Degradation of signal timing in cortical areas V1 and V2 of senescent monkeys. *Cereb. Cortex N. Y. N 1991* **15,** 403–408 (2005).
14. Onofrj, M., Thomas, A., Iacono, D., D'Andreamatteo, G. & Paci, C. Age-related changes of evoked potentials. *Neurophysiol. Clin. Neurophysiol.* **31,** 83–103 (2001).
15. Shaw, N. A. & Cant, B. R. Age-dependent changes in the latency of the pattern visual evoked potential. *Electroencephalogr. Clin. Neurophysiol.* **48,** 237–241 (1980).
16. Sokol, S., Moskowitz, A. & Towle, V. L. Age-related changes in the latency of the visual evoked potential: Influences of check size. *Electroencephalogr. Clin. Neurophysiol.* **51,** 559–562 (1981).
17. Tobimatsu, S. Aging and pattern visual evoked potentials. *Optom. Vis. Sci.* **72,** 192–197 (1995).
18. Iragui, V. J., Kutas, M., Mitchiner, M. R. & Hillyard, S. A. Effects of aging on event-related brain potentials and reaction times in an auditory oddball task. *Psychophysiology* **30,** 10–22 (1993).
19. Anderson, S., Parbery-Clark, A., White-Schwoch, T. & Kraus, N. Aging affects neural precision of speech encoding. *J. Neurosci.* **32,** 14156–14164 (2012).
20. Anderson, S., White-Schwoch, T., Parbery-Clark, A. & Kraus, N. Reversal of age-related neural timing delays with training. *Proc. Natl. Acad. Sci.* **110,** 4357–4362 (2013).
21. Bieniek, M. M., Frei, L. S. & Rousselet, G. A. Early ERPs to faces: aging, luminance, and individual differences. *Front. Psychol.* **4,** (2013).
22. Rousselet, G. *et al.* Age-related delay in information accrual for faces: Evidence from a parametric, single-trial EEG approach. **10,** (2009).
23. Rousselet, G. A. *et al.* Healthy aging delays scalp EEG sensitivity to noise in a face discrimination task. *Front. Psychol.* **1,** 19 (2010).
24. Chaby, L., George, N., Renault, B. & Fiori, N. Age-related changes in brain responses to personally known faces: an event-related potential (ERP) study in humans. *Neurosci. Lett.* **349,** 125–129 (2003).
25. Nakamura, A. *et al.* Age-related changes in brain neuromagnetic responses to face perception in humans. *Neurosci. Lett.* **312,** 13–16 (2001).
26. Spear, P. Neural bases of visual deficits during aging. *Vision Res.* **33,** 2589–2609 (1993).
27. Chaby, L., Jemel, B., George, N., Renault, B. & Fiori, N. An ERP study of famous face incongruity detection in middle age. *Brain Cogn.* **45,** 357–377 (2001).
28. Pfefferbaum, A., Ford, J. M., Roth, W. T. & Kopell, B. S. Age-related changes in auditory event-related potentials. *Electroencephalogr. Clin. Neurophysiol.* **49,** 266–276 (1980).
29. Pfütze, E.-M., Sommer, W. & Schweinberger, S. R. Age-related slowing in face and name recognition: evidence from event-related brain potentials. *Psychol. Aging* **17,** 140 (2002).
30. Hansen, J. C. & Hillyard, S. A. Endogeneous brain potentials associated with selective auditory attention. *Electroencephalogr. Clin. Neurophysiol.* **49,** 277–290 (1980).
31. Lopes da Silva, F. EEG and MEG: Relevance to neuroscience. *Neuron* **80,** 1112–1128 (2013).

32. Jensen, J. H., Helpern, J. A., Ramani, A., Lu, H. & Kaczynski, K. Diffusional kurtosis imaging: The quantification of non-gaussian water diffusion by means of magnetic resonance imaging. *Magn. Reson. Med.* **53,** 1432–1440 (2005).
33. Lu, H., Jensen, J. H., Ramani, A. & Helpern, J. A. Three-dimensional characterization of non-gaussian water diffusion in humans using diffusion kurtosis imaging. *NMR Biomed.* **19,** 236–247 (2006).
34. Falangola, M. F. *et al.* Age-related non-Gaussian diffusion patterns in the prefrontal brain. *J. Magn. Reson. Imaging* **28,** 1345–1350 (2008).
35. Henriques, R. N., Correia, M. M., Nunes, R. G. & Ferreira, H. A. Exploring the 3D geometry of the diffusion kurtosis tensor—Impact on the development of robust tractography procedures and novel biomarkers. *NeuroImage* **111,** 85–99 (2015).
36. Friston, K. *et al.* Multiple sparse priors for the M/EEG inverse problem. *NeuroImage* **39,** 1104–1120 (2008).
37. Taylor, A. B., MacKinnon, D. P. & Tein, J. Tests of the three-path mediated effect. *Organ. Res. Methods* (2007).
38. Pandya, D. N., Hallett, M. & Mukherjee, S. K. Intra- and interhemispheric connections of the neocortical auditory system in the rhesus monkey. *Brain Res.* **14,** 49–65 (1969).
39. Wessinger, C. M. *et al.* Hierarchical organization of the human auditory cortex revealed by functional magnetic resonance imaging. *J. Cogn. Neurosci.* **13,** 1–7 (2001).
40. Beauchamp, M. S., Lee, K. E., Argall, B. D. & Martin, A. Integration of auditory and visual information about objects in superior temporal sulcus. *Neuron* **41,** 809–823 (2004).
41. Gilbert, C. D. & Sigman, M. Brain states: top-down influences in sensory processing. *Neuron* **54,** 677–696 (2007).
42. Sussman, E., Winkler, I., Huotilainen, M., Ritter, W. & Näätänen, R. Top-down effects can modify the initially stimulus-driven auditory organization. *Cogn. Brain Res.* **13,** 393–405 (2002).
43. Selzer, M., Clarke, S., Cohen, L., Kwakkel, G. & Miller, R. *Textbook of Neural Repair and Rehabilitation: Volume 1, Neural Repair and Plasticity.* (Cambridge University Press, 2014).
44. Lindenberger, U., von Oertzen, T., Ghisletta, P. & Hertzog, C. Cross-sectional age variance extraction: what's change got to do with it? *Psychol. Aging* **26,** 34–47 (2011).
45. Shafto, M. A. *et al.* The Cambridge Centre for Ageing and Neuroscience (Cam-CAN) study protocol: a cross-sectional, lifespan, multidisciplinary examination of healthy cognitive ageing. *BMC Neurol.* **14,** (2014).
46. Taylor, J. R. *et al.* The Cambridge Centre for Ageing and Neuroscience (Cam-CAN) data repository: Structural and functional MRI, MEG, and cognitive data from a cross-sectional adult lifespan sample. *NeuroImage* (2015). doi:10.1016/j.neuroimage.2015.09.018
47. Nolte, G., Fieseler, T. & Curio, G. Perturbative analytical solutions of the magnetic forward problem for realistic volume conductors. *J. Appl. Phys.* **89,** 2360–2369 (2001).

*Cam-CAN corporate author list:*

The Cam-CAN corporate author consists of the project principal personnel: Lorraine K Tyler, Carol Brayne[5], Edward T Bullmore[5], Andrew C Calder[5], Rhodri Cusack[5], Tim Dalgleish[5], John Duncan[5], Richard N Henson[5], Fiona E Matthews[5], William D Marslen-Wilson[5], James B Rowe[5], Meredith A Shafto[5]; Research Associates: Karen Campbell[5], Teresa Cheung[5], Simon Davis[5], Linda Geerligs[5], Rogier Kievit[5], Anna McCarrey[5], Abdur Mustafa[5], Darren Price[5], David Samu[5], Jason R Taylor[5], Matthias Treder[5], Kamen A Tsvetanov[5], Janna van Belle[5], Nitin Williams[5]; Research Assistants: Lauren Bates[5], Tina Emery[5], Sharon Erzinglioglu[5], Andrew Gadie[5], Sofia Gerbase[5], Stanimira Georgieva[5], Claire Hanley[5], Beth Parkin[5], David Troy[5]; Affiliated Personnel: Tibor Auer[5], Marta Correia[5], Lu Gao[5], Emma Green[5], Rafael Henriques[5]; Research Interviewers: Jodie Allen[5], Gillian Amery[5], Liana Amunts[5], Anne Barcroft[5], Amanda Castle[5], Cheryl Dias[5], Jonathan Dowrick[5], Melissa Fair[5], Hayley Fisher[5], Anna Goulding[5], Adarsh Grewal[5], Geoff Hale[5], Andrew Hilton[5], Frances Johnson[5], Patricia Johnston[5], Thea Kavanagh-Williamson[5], Magdalena Kwasniewska[5], Alison McMinn[5], Kim Norman[5], Jessica Penrose[5], Fiona Roby[5], Diane Rowland[5], John Sargeant[5], Maggie Squire[5], Beth Stevens[5], Aldabra Stoddart[5], Cheryl Stone[5], Tracy Thompson[5], Ozlem Yazlik[5]; and administrative staff: Dan Barnes[5], Marie Dixon[5], Jaya Hillman[5], Joanne Mitchell[5], Laura Villis[5].